ModelMap: A Model-based Multi-domain Application Framework for Centralized Automotive Systems

Soham Sinha
soham1@bu.edu
Boston University
Boston, MA, USA

Anam Farrukh
afarrukh@bu.edu
Boston University
Boston, MA, USA

Richard West
richwest@bu.edu
Boston University
Boston, MA, USA

ABSTRACT

This paper presents *ModelMap*, a model-based multi-domain application development framework for DriveOS, our in-house centralized vehicle management software system. DriveOS runs on multicore x86 machines and uses hardware virtualization to host isolated RTOS and Linux guest OS sandboxes. In this work, we design Simulink interfaces for model-based vehicle control function development across multiple sandboxed domains in DriveOS. ModelMap provides abstractions to: (1) automatically generate periodic tasks bound to threads in different OS domains, (2) establish cross-domain synchronous and asynchronous communication interfaces, and (3) handle USB-based CAN I/O in Simulink. We introduce the concept of a *nested binary*, for the deployment of ELF binary executable code in different sandboxed domains. We demonstrate ModelMap using a combination of synthetic benchmarks, and experiments with Simulink models of a CAN Gateway and HVAC service running on an electric car. ModelMap eases the development of applications, which are shown to achieve industry-target performance using a multicore hardware platform in DriveOS.

CCS CONCEPTS

• **Software and its engineering → Integrated and visual development environments**.

KEYWORDS

multi-domain Simulink models, vehicle control software

ACM Reference Format:
Soham Sinha, Anam Farrukh, and Richard West. 2022. ModelMap: A Model-based Multi-domain Application Framework for Centralized Automotive Systems. In *IEEE/ACM International Conference on Computer-Aided Design (ICCAD '22), October 30-November 3, 2022, San Diego, CA, USA.* ACM, New York, NY, USA, 9 pages. https://doi.org/10.1145/3508352.3549463

1 INTRODUCTION

Automotive systems are continuing to increase in complexity, with the advent of advanced driver assistance systems and connected services. This has led to a corresponding increase in electronic control units (ECUs), with a modern luxury vehicle having over 100 such units [42]. An alternative approach to using large numbers of separate ECUs is to develop a centralized vehicle management system (VMS) [6] where functions are consolidated as software tasks on a single multicore machine [55]. Software is more easily upgraded and extended, without the cost of added electronics [23]. However, software tasks must now implement functions with different timing, safety and security requirements on the same hardware.

To address this, VMSs assign tasks having a high criticality, or consequence of failure, to a real-time OS (RTOS), while low criticality tasks run on a general purpose OS (GPOS) [1, 3, 7, 24, 41, 55]. Example high criticality tasks are those that affect vehicle control, including steering, throttle and braking, while low criticality tasks include infotainment services. Both the RTOS and GPOS are able to run on a single hardware platform using machine virtualization.

A significant challenge is how to develop, deploy and support communication between *mixed-criticality* tasks running in different domains, or operating systems, on multicore VMSs. To date, most vehicle functions such as heating, ventilation and air conditioning (HVAC) or powertrain control are developed for simple, single-core ECUs. These ECUs host a single, simple RTOS or firmware. Engineers accustomed to model-based design languages such as Simulink [21] and LabView develop functions for these ECUs without awareness of control flow (e.g., threads), data structures, and low-level communication primitives. Model-based design languages have thus far lacked support for multi-OS domain systems, leaving the burden on expert programmers to port ECU functions.

We introduce ModelMap, a **model**-based **m**ulti-domain **app**lication development framework for automotive functions in our in-house centralized VMS, called DriveOS. DriveOS leverages a partitioning hypervisor to host RTOS and Linux sandboxed domains on top of a multicore PC-class x86 machine [55]. ModelMap implements a set of Simulink interfaces that target multiple sandboxes, or OS-level protection domains, in DriveOS.

ModelMap supports binding a real-time periodic thread to a Simulink control task for timing-predictable execution. It provides synchronous and asynchronous inter-task communication primitives, and real-time I/O for commonly used protocols such as controller area network (CAN) bus. Vehicle functions that span OS domains are encapsulated as *nested binaries*, which support the deployment of executable code for multiple application binary interfaces. To the best of our knowledge, ModelMap is the first open model-based multi-domain VMS application framework.

We present two Simulink automotive software models and implement them using ModelMap Simulink blocks in DriveOS. These models are: (1) a CAN Gateway service, which delivers CAN messages to different software threads in DriveOS, according to end-to-end timing guarantees, and (2) a port of an HVAC controller for an electric vehicle being developed with our partner company. We demonstrate the HVAC model's functional and timing correctness with a model-in-the-loop (MIL) and hardware-in-the-loop (HIL) execution equivalence against real-world data traces.

The **contributions** of this paper are three-fold: (1) we introduce the first model-based multi-domain application development and deployment framework for a VMS; (2) we demonstrate that Simulink models running on a multicore x86-based centralized VMS have predictable end-to-end delays; (3) we illustrate a Simulink model's functional and timing correctness with MIL and HIL equivalence.

The next section provides motivation and background to model-based design in DriveOS. Section 3 describes the ModelMap tools for multi-domain code development. Section 4 explains the nested binary concept in the DriveOS VMS. An evaluation of ModelMap is covered in Section 5, using simulated and real-world data sets as well as CAN Gateway and HVAC case studies. This is followed by related work and conclusions, respectively, in Sections 6 and 7.

2 MOTIVATION AND BACKGROUND

Simulink Model-based Design. MATLAB/Simulink is the de-facto design tool for model-based vehicle control software. Proprietary functional blocks are commonly provided by vendors for use on their own ECUs, which traditionally feature single-core microcontrollers. However, the growing popularity of embedded multicore processors has led to the development of task-parallel Simulink models [5, 44, 45]. Notwithstanding, there appears to be a lack of Simulink model-based design frameworks for multi-OS domain systems. This has consequently motivated our work, which targets the use of Simulink development tools in hypervisor-based [13, 50, 58] vehicle management systems.

In Simulink, a control task is modeled with a number of functional blocks that are connected with signals. Each functional block derives output signals from a combination of its inputs and internal states. A *subsystem* comprises one or more functional blocks.

A complete control system is developed from multiple subsystems. In a modern VMS, these subsystems may require execution in different OS domains, depending on criticality and functionality. For example, a CAN Gateway [55] might run within an RTOS to directly access a timing- and security-critical vehicle bus for chassis and powertrain control. At the same time it may wish to transfer processed data from the CAN bus via secure shared memory to a Linux domain, to update a less critical instrument cluster service that relies on a graphical display. Likewise, a Linux domain user-interface to control cabin temperatures might interact with an HVAC controller within an RTOS. ModelMap eases the development of applications for these types of multi-domain systems.

Centralized VMS. A centralized VMS consolidates multiple ECU functions onto a multicore platform. Drako Motors' DriveOS™ [54, 55], Mercedes-Benz' MB.OS [41] and Toyota's Arene OS [1] are examples of centralized VMSs. These all support multiple guest operating systems, or sandbox domains, running on a partitioning hypervisor [46, 58]. They provide temporal and spatial isolation between guest sandboxes so that tasks executing within one sandbox do not interfere with tasks in other sandboxes. The hypervisor is removed from normal sandbox execution, allowing guest operating systems to execute directly on their assigned hardware.

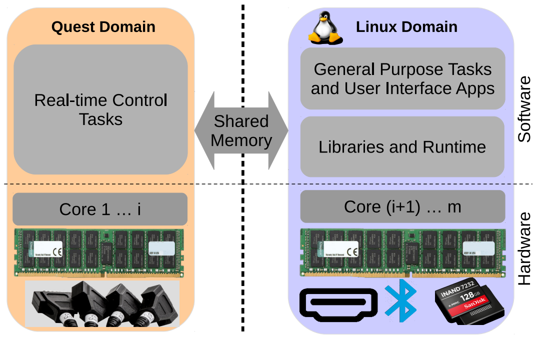

Figure 1: High-level Design of DriveOS

This paper addresses the tools and mechanisms for multi-domain functional development and deployment, in the context of DriveOS, as shown in Figure 1. A Quest real-time OS [14] domain works in unison with a general-purpose Linux OS domain. For proof of concept, this paper focuses on two single-core domains, although DriveOS is capable of supporting more domains and cores.

3 ModelMap DESIGN TOOLS

Figure 2 shows an overview of the ModelMap code generation for a multi-domain application. A model is first designed with ModelMap and other Simulink blocks. Then, ModelMap block-level and DriveOS system Target Language Compiler (TLC) [53] files are utilized by the Simulink Embedded Coder, to generate the domain OS-specific C source code. OS-specific versions of `gcc` cross-compile C code into Quest and Linux ELF binaries. Finally, a nested binary compiler (see Section 4) creates a multi-domain binary executable.

A custom Embedded Real-Time (ERT) system TLC file [53] specifies the C code generation from Simulink model blocks. This is explained further in Section 3.1.4.

3.1 Thread Setup Blocks

A `threadSetup` Simulink block is used to create periodic threads for either Quest or Linux, and aperiodic threads restricted to Linux. The block details are summarized below:

- **Block Type:** C MEX S-function [34].
- **Block Parameters:** A Simulink block mask [35] identifies thread-specific parameters. These include the *Thread Name* and *Domain* OS (Quest or Linux). A Quest periodic thread is further parameterized with a *Runtime* and *Period*. A Linux domain periodic thread has a *Runtime*, *Period* and *Deadline*, while a Linux-only aperiodic thread has no further parameters.

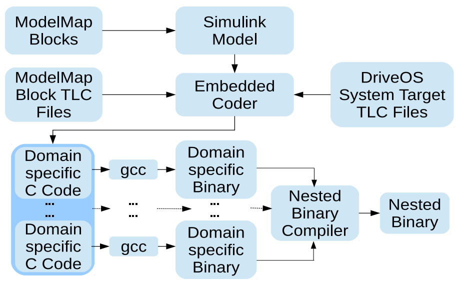

Figure 2: The ModelMap Workflow

• **Block Output:** The output of this block is a function trigger signal that connects to an input trigger port of a *function-call subsystem* [39]. This subsystem is executed as a threaded task configured using the above parameters.

3.1.1 *Quest Periodic Threads.*

Timing and safety critical control tasks run as periodic threads in Quest. Application threads in this domain leverage Quest-specific and C library [43] APIs, to perform real-time I/O and secure CAN bus operations.

Example tasks include HVAC and powertrain control, which are designed as Simulink function-call subsystems. The function trigger ports of these subsystems are connected to the output port of a corresponding threadSetup block. threadSetup is configured with a *Thread Name* parameter, and the *Domain* is set to Quest. A model developer provides the *Runtime* and *Period* parameters that are respectively set as the *budget* (C) and *period* (T) of a Quest periodic task, τ. τ is implemented following a Liu-Layland task model and scheduled using the RMS algorithm [30]. This guarantees τ receives its budget, C, every period, T, when runnable.

3.1.2 *Linux Periodic Threads.*

Linux is the lower criticality GPOS domain in DriveOS. Although not a hard real-time OS, it provides sufficiently predictable timing guarantees for SCHED_DEADLINE [27] tasks using the PREEMPT_RT patch [47]. Linux provides complementary support for Quest with its libraries, device drivers and services that would take many years of development to implement in a new RTOS. A developer provides the *Runtime*, *Period* and *Deadline* threadSetup block parameters that are passed on to the SCHED_DEADLINE policy via the Linux sched_setattr system call.

3.1.3 *Linux Aperiodic Threads.*

A centralized VMS also runs non-timing critical operations such as logging, storage and over-the-air updates. threadSetup supports these tasks as Linux pthreads. No additional threadSetup block parameters are needed.

3.1.4 *Code Generation.*

The threadSetup S-function block's properties are described in a C MEX (threadSetup.c) file for simulation, and in a TLC file (threadSetup.tlc) for code generation. As the threadSetup block is designed for model deployment in a DriveOS system, threadSetup.c only saves the block parameters for code generation, without any simulation. In the threadSetup.tlc file, three key steps are followed to generate its corresponding C code [32]:

1) The BlockInstanceSetup TLC function of an S-function block is executed at the very start of code generation. ModelMap uses this function to retrieve all the block parameters from the simulation environment.

2) The Start TLC function (Code Block 1) includes any initializing code in the final C source code. ModelMap uses this function to assign the block parameters (*Runtime*, *Period* and, if applicable, *Deadline*) to a DriveOS C structure (driveos_sched_param_t) with domain-specific members.

```
%% Simulink TLC Code starts with a %; TLC comments start with a %%
%% Any other code goes to an initializing block of the final C code
%if targetosVal == 0 %% Quest domain
  s_params->C = %<Quest budget>; s_params->T = %<Quest period>;
%elseif linuxschedpolicyVal == 1 %% Linux domain SCHED_DEADLINE
  s_params->is_sched_deadline = 1; s_params->C = %<linuxruntime>;
  ...
%endif
s_params->threadfuncname = %<threadName>_func;
```

Code Block 1: A snippet of the Start TLC function

The DriveOS system TLC file declares all_thrd_parms as an array of driveos_sched_param_t structures. This array is used to save the parameters of multiple threads in the same domain, each time a Start function of a threadSetup block is called.

3) The Output TLC function of a block is used to generate the block's corresponding C code. ModelMap uses Output to add a new function in the model's C source file, named <threadName>_func. The same function is also embedded in the previous Start function as the pthread function name. The driveos_sched_param_t C structure is passed as an argument to the pthread function, to set the corresponding thread scheduling parameters for the given domain. Finally, a %<LibBlockExecuteFcnCall>() TLC function is embedded in an infinite while loop, to repeatedly invoke the subsystem's corresponding C function according to the specific scheduling parameters.

The DriveOS system TLC spawns the pthreads from the main function of the generated C source code. A Simulink custom file processing template [36] is used to generate the main function. A new pthread is created for every element in all_thrd_parms. Part of the main function is shown in Code Block 2.

```
for(i = 0; i < num_threads; i++) {
#ifdef QUEST
  pthread_t* new_thread = (pthread_t *) malloc(sizeof(pthread_t));
  pthread_create(new_thread, NULL, all_thrd_parms[i].threadfuncname,
        all_thrd_parms[i]);
#else
// Linux domain
  ...
#endif
}
```

Code Block 2: A snippet of the ModelMap-generated main function in C

3.2 Inter-task Communication Blocks

ModelMap provides a set of blocks for intra- and inter-domain task communications. These blocks are set up as *shared memory communication channels* by the DriveOS hypervisor [55]. Intel VT-x extended page tables (EPTs) securely map host physical memory regions between communicating threads, irrespective of their domain. Both synchronous and asynchronous communications are supported across channels identified with a unique channel_key.

DriveOS has a set of C API functions in Linux and Quest to set up the communication channels. ModelMap implements MATLAB interfaces for these C functions [33], which are described below.

A ModelMap createChannel Simulink block takes an integer input as the channel_key. It has block mask parameters to set the type and specification of the channel. For a synchronous channel, the buffer length and the size of each element must be specified. For an asynchronous channel, only the element size is needed.

3.2.1 *Synchronous Communication.*

A synchronous channel is implemented as a ring buffer in DriveOS. This is useful for control data that must be communicated without loss. Channel data structures are created by OS-specific userspace libraries in both Quest and Linux domains. syncRead and syncWrite are busy-waiting calls that read and write, respectively, a message in the buffer. Busy-waiting is used for synchronous communication in Quest-V [58] and DriveOS [55].

Blocking or busy-waiting is problematic when reading or writing to different channels. As will be seen later in Figure 10, a syncRead on one channel may delay the execution of syncRead calls on other channels. To mitigate this issue, ModelMap implements syncNWRead and syncNWWrite, which are non-waiting (NW) functions. Calling syncNWRead (or syncNWWrite) when a channel buffer is empty (or full) immediately returns -1, otherwise it returns the size of the read (or written) message.

3.2.2 Asynchronous Communication. An asynchronous channel in DriveOS is implemented using Simpson's four-slot protocol [52]. This is useful when the most recent (i.e., freshest) data must be communicated, while stale data is discarded. Sensor readings fall into this category of communication. The `asyncRead` and `asyncWrite` Simulink blocks are available to read and write asynchronous messages, respectively.

3.3 CAN I/O Blocks

CAN communication between sensors and actuators is commonly used in the automotive domain. DriveOS implements real-time USB-CAN I/O in its Quest domain. The Quest CAN I/O API is accessed via MATLAB's C-interface function blocks, including `canChannelSetup`, `canRead`, and `canWrite`. `canChannelSetup` has a block parameter to set the CAN baud rate from 10 kbit/s to 1Mbit/s.

3.4 Timing Blocks

ModelMap implements several Simulink timing blocks. MATLAB function block `time_from_start` outputs the time in μs since the model starts running. Similarly, `time_since_last_called` outputs the time in μs since the last time this block was called. These timing functions use the x86 `RDTSC` instruction to measure processor clock cycles, divided by the base clock frequency, to yield accurate time in μs. These blocks are C-function interfaces in MATLAB [33].

3.5 Domain-specific C Code Generation

Domain-specific components of a model are designed as subsystems in Simulink. The `slbuild(<subsystem name>)` command is used by ModelMap to generate domain-specific C code for a target Simulink subsystem.

4 NESTED BINARIES

ModelMap produces an ELF binary [31] format for DriveOS, called a *nested binary*. This is similar to a fat binary [17], and contains multiple executables with Application Binary Interfaces (ABIs) for different operating systems. For example, DriveOS nested binaries contain executable images for both Quest and Yocto Linux.

ModelMap includes a nested binary compiler. A corresponding nested binary loader performs runtime parsing of individual executables within a nested binary. It then spawns a new process for every executable into a corresponding DriveOS sandboxed domain.

4.1 Nested Binary Format

As shown in Figure 3, a nested binary section header table contains file offsets to $N \geq 1$ `binexec` sections. Each `binexec` section stores the ELF binary data for a specific domain executable. A nested binary `metadata` ELF section also stores the mapping between an individual ELF binary and a runtime domain ID.

4.1.1 ELF Header. The ELF header defines the target OS ABI, bitness, and other details in an ELF binary. The following fields are modified: (1) **`e_ident[EI_OSABI]`:** The target OS ABI is set to a custom value of `0x15`; (2) **`e_machine`:** The target ISA is set to `EM_386` (`0x03`) for an x86 target; (3) **`e_type`:** The object file type is set to `0x02` for an executable file; (4) **`e_ident[EI_DATA]`:** The endianness is set to little-endian.

4.1.2 Program Header Table. This section has one entry to satisfy the ELF format requirement. The entry is the Program Header Table

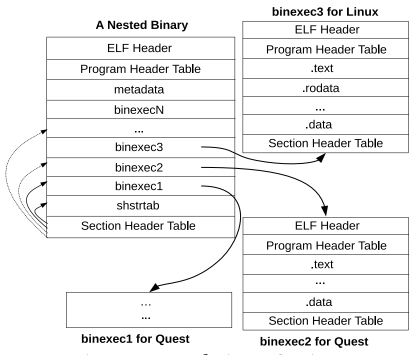

Figure 3: Nested Binary Sections

(`PT_PHDR`) itself. As individual executables have their own program header information, this section is not needed.

4.1.3 Section Header Table. This section lists all the data sections in a nested binary:

- **`binexec`:** Every nested binary has a separate `binexec` section for each ELF binary executable. The name of every `binexec` section is appended at the end with an integer numeric ID, starting from 1. This ID specifies the order in which the binaries will be spawned at runtime, where lower ID means earlier execution.
- **`metadata`:** The `metadata` section maps an individual binary in a `binexec` section to a domain in DriveOS. The nested binary loader uses the metadata section to spawn a new process from an individual binary in the corresponding domain. The section contains an array of `C structs` which holds a tuple of the `binexec` section name and the corresponding integer domain ID. Currently, DriveOS assigns domain ID 1 to Quest and 2 to Linux.
- **`shstrtab`:** This is the string table section that contains the section names, like other ELF binaries.

4.2 Nested Binary Compiler

ModelMap's nested binary compiler (`nested_bin_cc`) creates a nested ELF binary from multiple individual binary executable files. The compiler utilizes the `libelf` library [25] to create, enumerate and organize different ELF binary sections according to the above format. The following command is used to create a nested binary:

```
nested_bin_cc <Binary File1> <Domain ID1> ...
        <Binary FileN> <Domain IDN> <Name of Nested Binary>
```

The above command combines N ELF binary executable files and saves the mapping between a binary and its runtime domain in the `metadata` section. For example, `Binary File1` is mapped to `Domain ID1`. A new nested binary is created with the name specified in the last argument. `binutils` tools such as `readelf` support inspection of nested binary sections.

4.3 Nested Binary Loader

The nested binary loader is also implemented with the `libelf` APIs [25]. The loader runs in a DriveOS Linux domain and takes a nested binary as the first argument. It also takes a number of command-line arguments for every individual ELF binary. The following command is used to execute a nested binary:

```
nested_loader <nested ELF binary>
        <argc1> <argv11> ... <argc2> <argv21> ...
```

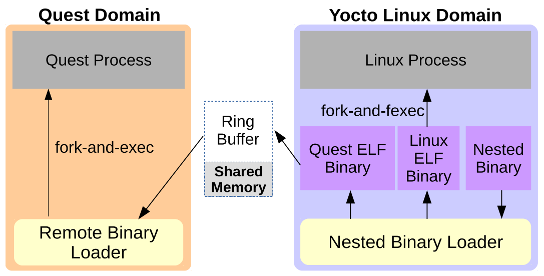

Figure 4: Nested Binary Loader

Here, `argc1` is the number of command-line arguments for the `binexec1`, starting with `argv11`. Similarly, `argc2` is the argument count for `binexec2`, starting with `argv21`, and so on.

The loader parses the `metadata` section in a nested binary to read the mapping between a `binexec` section and its runtime domain. It spawns a new process with the raw bytes of a binary embedded in a `binexec` section to its respective domain. Figure 4 summarizes the steps to execute a binary in Linux and Quest.

4.3.1 Executing a binary in a Linux Domain. The nested binary loader parses the metadata section of a target binary to locate the corresponding `binexec` sections for Linux (Domain ID=2). The loader employs the fork-and-exec approach in Linux to spawn the executable image as a new process. However, as the executable is not in a file and directly available in memory, the `execve`-class of `C` functions cannot be used. Instead, the loader creates a new file descriptor for the memory location of the Linux binary with the `memfd_create` function [29]. Then, it `forks` a new child process and calls `fexecve` [28] to start execution.

4.3.2 Executing a binary in a Quest Domain. In this case, the Linux nested binary loader first identifies the domain ID=1 for a Quest binary object. It then sends the executable bytes to Quest via shared memory as shown in Figure 4. A specific shared memory region of 800KB is mapped between the Quest and Linux domains at system boot time for remote binary execution. The region is appropriately sized to accommodate typical Quest static binaries. This shared memory region works as a synchronous ring buffer channel with a single buffer slot. A remote binary loader process in Quest polls the shared region for any new binary execution request. Once the Linux nested binary loader indicates that it has written a new program to the shared region, the remote binary loader in Quest starts reading the program and its arguments. Then, the remote Quest loader spawns a new process with a fork-and-exec mechanism.

5 EVALUATION

In this section, ModelMap is tested with custom and real-world Simulink models. The goal is to show that the end-to-end (E2E) delays, or the maximum reaction times [15], of the models are within their expected upper bounds after deployment in DriveOS.

ModelMap Simulink blocks are applied to the following three models: (1) a multi-domain *synthetic benchmark* with different types of inter-task communication, (2) a DriveOS *CAN Gateway* [56] to filter and forward CAN messages to different Quest and Yocto Linux applications, and (3) a port of an *automotive HVAC* Simulink model for a MotoHawk ECU to the DriveOS VMS. The functional and timing correctness of the ported HVAC model is demonstrated by the output equivalence in both MIL and HIL execution.

The three models are tested with the DriveOS VMS running on a Cincoze DX1100 industrial PC [12], featuring an Intel 2.4GHz i7-8700T processor. The DX1100 is connected to a Kvaser Pro 5xHS USB-CAN adapter [26].

DriveOS supports real-time USB-based CAN I/O using Quest. Quest handles device interrupts in the context of *time-budgeted, schedulable threads* [14]. The test setup uses two USB xHCI bottom-half handler threads, each with budget=0.1ms and period=1ms, referred to as `USBBH_rx` and `USBBH_tx`. Two USB-CAN kernel driver threads, each with budget=0.2ms and period=1ms, send (`CAN_tx`) and receive (`CAN_rx`) CAN messages.

5.1 Synthetic Benchmarks

Figure 5 shows our multi-domain Simulink benchmark model, designed using ModelMap blocks. The inter-task and CAN channel setup blocks are not shown for space constraints. The model reads a CAN message in the `canReader` subsystem of the Quest domain (Domain 1) from CAN channel 0 (CAN0) via `canRead`. Then, `syncWrite` forwards the data to the `procThread` subsystem for processing in the Linux domain (Domain 2). This setup allows `procThread` to apply any control logic to the received message using additional Simulink blocks. For our experiments, `procThread` forwards the message to a `canWriter` subsystem in Domain 1 using `syncWrite`. The `canWriter` then outputs a message on CAN channel 1 (CAN1). This model is representative of the canonical communication path between two CAN bus interfaces and separate OS domains in DriveOS.

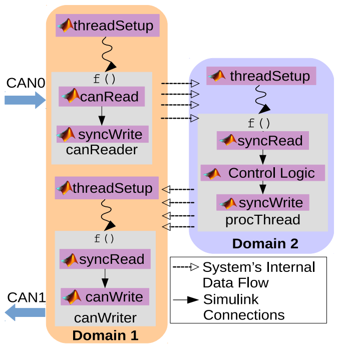

Figure 5: A Multi-Domain Simulink Benchmark

The `canReader`, `canWriter` and `procThread` blocks in Figure 5 are function-call subsystems, configured as periodic threads. Their function trigger ports are connected to the output ports of the `threadSetup` blocks. The `threadSetup` blocks are assigned to the Quest domain for the `canReader` and `canWriter` subsystems, and to the Linux domain for the `procThread` subsystem. Their budgets and periods, given in Table 1, are derived empirically by profiling [59], and assigned in the corresponding `threadSetup` blocks. `canReader` and `canWriter` subsystems rely on Quest real-time capabilities. `procThread` is representative of a lower criticality control task that is scheduled in the Linux domain using the `SCHED_DEADLINE` policy.

The Simulink model's corresponding C code and subsequent nested binaries are automatically generated. When this model is launched by ModelMap's nested binary loader, `canReader` and `canWriter` threads are spawned in Domain 1, and `procThread` is

Table 1: Budgets and Periods for the Synthetic Benchmark

Subsystem/Thread	Budget (μs)	Period (μs)	Util. (%)	# of Threads
Domain 1				
canReader	100	2000	5%	1
canWriter	100	2000	5%	1
Domain 2				
procThread	100-500	1000	10-50%	1

spawned in Domain 2 at runtime. This model is a classic example of a sensing-processing-actuation task pipeline [2, 15].

5.1.1 End-to-end Delay Performance. We measure the end-to-end (E2E) delay (also known as the maximum reaction time) [11, 15, 18] of a CAN message traversing through `canReader` → `procThread` → `canWriter` threads. The E2E delay upper bound for a pipeline of periodic real-time tasks has been theoretically analyzed before [2, 15, 18], but only for a domain-specific scheduling algorithm. However, it is important to measure the E2E delay of multi-domain applications in a centralized VMS where the time-critical software components expand beyond a single domain [3, 55]. We perform an experimental evaluation of such multi-domain applications in this paper and use the sum of the task periods [22] (*optimistic*) and Davare's upper bound [15] (*conservative*, twice the sum of periods assuming response-time of a task ≤ its period) as the two target E2E delay bounds. As stated earlier, the `USBBH_rx`, `USBBH_tx`, `CAN_rx` and `CAN_tx` threads are also considered in a task chain for CAN I/O, as a CAN message has to pass through these I/O threads as well. For example, the aggregate period delay bound for Figure 5 will be ((1 + 1 + 1 + 1) [for the I/O system threads] + (2 + 2 + 1) [from Table 1]) = 9ms.

5.1.2 Result Analysis. A stream of messages is sent from an Ubuntu 18.04 Linux machine to DriveOS via CAN0 on the DX1100. A corresponding message is received via CAN1 on the same Ubuntu machine. The sent and received CAN message timestamps are logged with `candump` in Ubuntu, to calculate the E2E delay. In the first set of experiments, we vary the utilization (ratio of *Runtime* and *Period*) of the `procThread` subsystem from 10 to 50% by increasing the *Runtime* parameter in the associated `threadSetup` block. Figure 6a shows the minimum, average and maximum E2E delays with increasing `procThread` utilization in Linux. All the E2E delays are within the target upper bounds.

Figure 6a shows that the maximum E2E delay is improved by 46%, as `procThread`'s utilization is increased from 10% to 50% in Linux. This coincides with the increased fraction of all E2E delays within the x-axis bound in Figure 6b. The median latency every 10 frames in Figure 7 is more variable for the 10% case than others. Allocating more utilization to a Linux domain subsystem not only improves the maximum E2E delay but also reduces jitter. However, CPU utilization is often limited in resource-constrained automotive systems. ModelMap's maximum E2E guarantee is crucial for time-critical control software modeling.

5.1.3 `procThread` in RTOS vs. Linux. The next experiment compares the previous model to one where the `procThread` subsystem in Figure 5 is moved to Domain 1, leaving Domain 2 idle. A special *BG* scheduling mode in Quest is also tested. This mode gives additional CPU time to a task beyond its model-specified CPU time via *background scheduling*, if other tasks do not need anymore CPU.

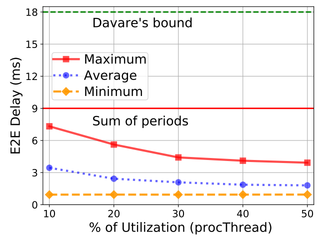

(a) Average, Minimum, Maximum

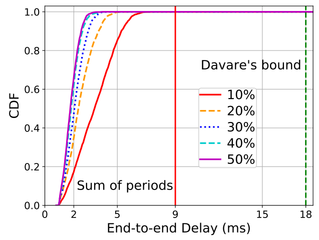

(b) Cumulative Distribution Function

Figure 6: Benchmark E2E Delay vs Domain 2 Task Utilization

Figure 9a shows the E2E delays when increasing the `procThread` utilization up to 30% [1], keeping its period fixed at 1ms. All E2E delays are under the target upper bounds. The maximum E2E delays for the Quest *BG* mode stay almost the same, as `procThread` leverages additional CPU time. Disabling *BG* mode still yields E2E delays under the target bounds, but the maximum ones are worse than Linux for higher utilization. As `procThread`'s period is fixed, its priority remains the same in Quest, even with higher utilization. Therefore, the maximum E2E delay does not decrease as much as it does while running in Linux, where only `procThread` is executed.

In another experiment, `procThread`'s period is increased from 1ms to 8ms, keeping its utilization fixed at 10%. The results in Figure 9b show that the E2E delays are increased with greater `procThread` period. If a CAN message is not handled in the same job (i.e., task instance) that it is received, it might wait for potentially more than a task's period to be transferred. Therefore, E2E delays increase with higher `procThread` periods. However, the maximum E2E delays are within the target upper bounds, except for the 8ms period in Linux where it violates the aggregate period bound. As the `procThread` period in the 8ms case is significantly more (4x) than the periods of `canReader` and `canWriter` threads (2ms), buffering delays increase the maximum E2E delay beyond the sum of periods. Nevertheless, all the delays are well under Davare's bound.

5.1.4 Asynchronous Communication Block. The next experiment replaces all `syncRead` (and `syncWrite`) blocks with `asyncRead` (and

[1] >30% is not possible due to the rate-monotonic scheduling bound with other tasks.

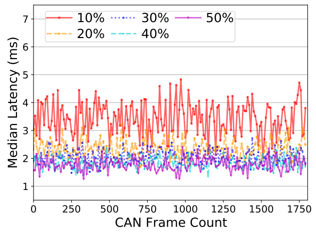

Figure 7: Synthetic Benchmark

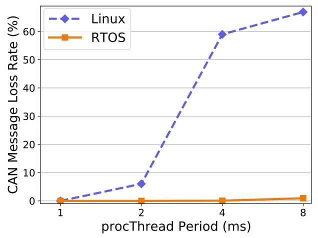

Figure 8: Loss Rate in Async Channel

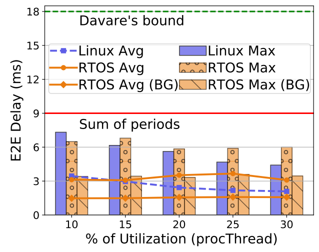

(a) Increasing Util. (Fixed Period)

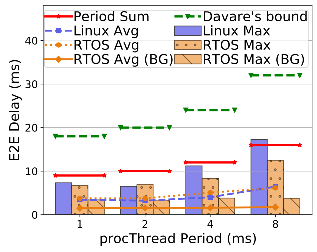

(b) Increasing Period (Fixed Util.)

Figure 9: Running procThread in Linux (Domain2) vs. RTOS (Domain1)

`asyncWrite`) blocks in the model of Figure 5. In asynchronous communication, if a receiver task has a greater period than a sender task, then a message is potentially overwritten by the sender, before it is observed by the reader. The number of lost messages is important in asynchronous communications. Figure 8 shows the loss-rate (ratio of number of lost messages and total messages) against increasing `procThread` period, while it is run in Linux and Quest.

A stream of 1275 CAN messages are sent at 5ms intervals from the Ubuntu machine. In Figure 8, as long as receiving `procThread`'s period in Linux is less than the sending `canReader`'s period of 2ms, there is no data loss. The loss-rate increases with greater periods from 2ms. As `procThread`'s period goes greater than or equal to `canReader`'s period, `procThread` starts missing CAN messages. In the Quest-only model, no loss is observed until 8ms period, because the source message rate (1/5ms=200Hz) is greater than the rate of all the tasks, and they are all running with the same RMS scheduling policy. However, when `procThread` runs in Linux it is scheduled earliest-deadline first according to the `SCHED_DEADLINE` policy. As Quest tasks are scheduled in RMS order there is a potential priority mismatch, highlighting the importance of correctly setting task periods for multi-domain task models.

5.2 Case Study 1: CAN Gateway

DriveOS's CAN Gateway is shown as a ModelMap Simulink model in Figure 10. It is used to distribute messages between different domains and CAN buses.

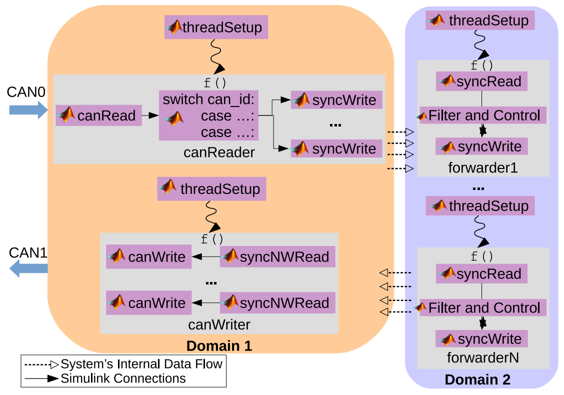

Figure 10: Model of a CAN Gateway

As before, CAN messages are read via CAN0 in Quest (Domain 1) and forwarded to Linux (Domain 2) by a `canReader` subsystem. A `canWriter` subsystem receives CAN messages from Linux to be sent out via CAN1. Unlike the previous benchmark model, there are multiple subsystems in Linux to process different categories of CAN messages based on their CAN IDs.

Figure 10 shows N Linux subsystems (`forwarder{1...N}`) where $N = \{1, 2, 4, 8\}$ in our experiments. Each `forwarder` Linux subsystem is connected to two inter-task synchronous channels: one is to receive CAN messages from `canReader`, another is to send CAN messages to `canWriter`. If a different Linux application wants to receive (or send) a message of any particular CAN ID, it has to request it from the specific Linux `forwarder` subsystem of the CAN Gateway. For example, Instrument Cluster and In-vehicle Infotainment applications in DriveOS request CAN message transfers via specific Linux `forwarder` subsystems. For the E2E delay overhead

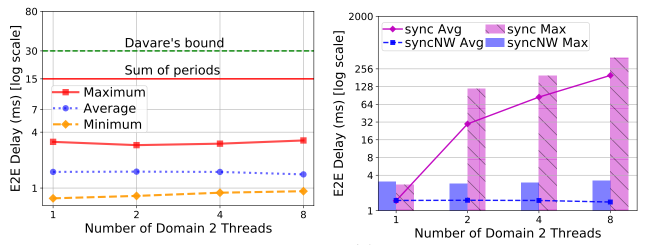

(a) Increasing # of Domain2 Threads **(b) Polling vs Non-polling Read**

Figure 11: CAN Gateway Case Study

of the CAN Gateway, `forwarder{1...N}` pass through the CAN messages from their incoming inter-task channel (from `canReader`) to the outgoing channel (to `canWriter`).

The `syncNWRead` block in `canWriter` is used to read from inter-task channels, without busy-waiting when a buffer is empty. Experiments show that `syncNWRead` significantly improves the E2E delay. `syncNWWrite` blocks are not used in `canReader`, as the Linux subsystems keep the inter-domain communication buffer free by reading out messages at a suitable rate.

Table 2: Budgets and Periods for CAN Gateway Case Study

Subsystem	Budget (μs)	Period (μs)	Util. (%)	# of Threads
		Domain 1		
canReader	200	2000	10%	1
canWriter	300	1000	30%	1
		Domain 2		
forwarder{1–8}	6400-800	8000 (fixed)	80%-10%	1-8

5.2.1 Result Analysis. Table 2 shows the budgets and periods of all the CAN Gateway tasks. The E2E delays are plotted in Figure 11 against increasing numbers of Linux `forwarder` threads, keeping their total utilization at 80%. For example, if two `forwarder` threads are executed, then each of them has 40% utilization. The E2E delays in Figure 11a exhibit low jitter and remain under the target bounds in all cases. This shows that ModelMap's CAN Gateway is able to handle multiple Linux threads in a DriveOS VMS system.

In other experiments, `syncNWRead`s are replaced with `syncRead` blocks in the `canWriter` subsystem. Figure 11b demonstrates that the polling `syncRead` block increases the E2E delay sharply as the number of threads increase. `syncNWRead` blocks are important for a scalable CAN Gateway as the busy-waiting times on synchronous channels are prohibitively large with more threads.

5.3 Case Study 2: Automotive HVAC Control

In this study, an HVAC controller running on a MotoHawk ECU is ported to DriveOS using ModelMap Simulink blocks. The HVAC Simulink function-call subsystem is connected to a `threadSetup` block. `threadSetup` configures the HVAC subsystem to run in the Quest domain with 0.5ms budget and 5ms period. The HVAC subsystem communicates with the Linux domain to save settings in persistent storage for when the vehicle is restarted. The functional and timing correctness of the HVAC control is investigated.

The HVAC control receives input signals via 18 CAN IDs and sends the output signals via 7 additional IDs. CAN I/O is via two inter-task communication channels with the CAN Gateway mentioned above. The HVAC control avoids waiting on any CAN IDs by using `syncNWWrite` and `syncNWRead` blocks for message transfers. The CAN Gateway `canReader` and `canWriter` threads are set to 0.2ms budget and 4ms period.

The HIL outputs of the HVAC model after its deployment in DriveOS are compared with the MIL outputs in Simulink, using CAN data traces from our electric car. Every CAN input message is tagged with a unique and monotonically increasing integer Tag ID, which is passed through to the HVAC control's output CAN messages. The HIL and MIL signal values in the HVAC control are checked to see that they match for all Tag IDs. Due to space limits, the HIL and MIL Driver Temperature signal outputs are shown over 30 seconds in Figure 12. For Tag IDs 756 and 762, `driv_temp` is respectively 1 and 2 in both MIL and HIL simulations. This is observed for all the Tag IDs and signals. The time difference on the x-axis is the DriveOS system and HVAC control overhead and contributes to the signal reaction time. Reaction times for all the signals in the HVAC control are in the similar range of 160–180 ms, which is deemed acceptable for our vehicle.

5.4 System Overheads

ModelMap overheads are measured with a series of microbenchmarks, averaged over 20 runs. The x86 `RDTSC` instruction is used for timing measurements, having an overhead of $0.04\mu s$ or ~96 clock cycles, which is subtracted from all delays.

Table 3: System Overheads for the DriveOS Simulink Blocks

	Time (μs)	
Simulink Block	**Linux**	**Quest**
threadSetup	33	190
channelCreate{Sender,Receiver}	5722	5486
channelConnect	5699	5448
(a)syncRead/Write	0.01-0.03	0.01-0.03
canChannelSetup	-	18490
canRead/Write	-	1

Table 3 presents the overheads of the ModelMap Simulink blocks in DriveOS. The `threadSetup` block takes more time in Quest than it takes in Linux, because Quest has to create a sporadic server abstraction for RMS [14, 57]. The creation and connection to an inter-task communication channel make expensive `VMExit` [46, 55] operations to the underlying hypervisor and take more time than reading/writing to the memory-mapped channels. CAN channel setup takes 18ms to configure the transfer rate of the USB-CAN interface. These blocks are only applied in an initial setup phase without significant runtime costs.

5.4.1 Nested Binary Measurements. A nested binary's size is the sum of all individual binaries and 14-bytes of metadata per binary.

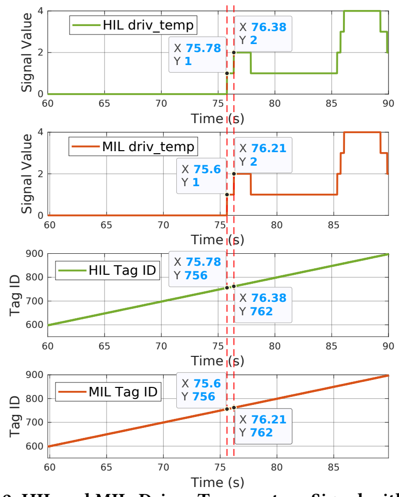

Figure 12: HIL and MIL: Driver Temperature Signal with Tag IDs

Table 4 presents the overheads of executing a nested binary. Quest only supports static binaries for fast and predictable runtime, so they are typically larger than Linux dynamically-linked binaries.

Table 4: Nested Binary Overheads

Operation	Time (ms)
Extracting an individual binary from a nested binary	0.16
Forking a process via memory in Linux	0.11
Sending ~300KB binary from Linux to Quest	7.13
Receiving ~300KB binary in Quest and forking it	184

6 RELATED WORK

Pagetti *et al.* have done extensive work on periodic Simulink models for multicore platforms based on the ROSACE architecture for avionics [5, 44, 45]. They employ formal verification techniques from design to code generation, to meet avionics standards. However, multicore CPU modeling and verified code generation remains a challenge, and relies on *faithful* code translation from other high-level formally defined design languages like Lustre.

Formal verification has been applied in the context of Simulink to C code generation [4], and is being used by automotive companies [21]. Other work has investigated design-level verification of Simulink models [9, 16, 19, 40, 48]. Fons-Albert *et al.* [20] applied model-based design to integrated modular avionics using the XtratuM hypervisor [13], focusing on application partitioning, automatic code generation and real-time tasking. However, little has been done on multi-domain code generation and deployment.

Emerging multi-domain vehicle management systems [1, 3, 41, 54, 55] require redesigned control function development tools [51]. Although new approaches are being considered [10, 49], they mostly target ECU-based systems [8]. In recent years, MathWorks has presented Simulink Desktop Real-time [37] for real-time simulation of models. However, it is not a VMS solution. Simulink now supports Linux and VxWorks [60] tasks, but without any periodic control mechanism [38]. ModelMap presents an end-to-end model-based framework for next-generation multi-domain VMS platforms.

7 CONCLUSIONS AND FUTURE WORK

This work presents ModelMap for model-based multi-domain application development and deployment in a centralized vehicle management system. ModelMap consists of Simulink blocks for binding real-time threads of control, inter-task communication and CAN I/O. It supports the generation of *nested binary* executables to encapsulate and execute DriveOS applications. Experiments show that custom and real-world DriveOS Simulink models, designed using ModelMap, have predictable end-to-end delays, in keeping with the requirements of a high performance electric vehicle.

Future work will use ModelMap to integrate additional vehicle control functions related to powertrain and battery management into DriveOS. Plans are underway to extend ModelMap interfaces with a model-driven pipeline programming language for multi-/manycore systems spanning multiple OS domains.

8 ACKNOWLEDGEMENTS

This work is supported in part by the National Science Foundation (NSF) under Grant # 2007707. Any opinions, findings, and conclusions or recommendations expressed in this material are those of the author(s) and do not necessarily reflect the views of the NSF. Special thanks are also given to our colleagues at Drako Motors.

REFERENCES

[1] Apex.ai. Customer Success Story: Toyota's Woven Planet, 2022. https://www.apex.ai/toyota-woven-planet.

[2] M. Becker, D. Dasari, S. Mubeen, M. Behnam, and T. Nolte. End-to-end Timing Analysis of Cause-effect Chains in Automotive Embedded Systems. *Journal of Systems Architecture*, 80:104–113, 2017.

[3] L. Belluardo, A. Stevanato, D. Casini, G. Cicero, A. Biondi, and G. Buttazzo. A Multi-Domain Software Architecture for Safe and Secure Autonomous Driving. In *Proceedings of the 27th IEEE RTCSA Conference*, 2021.

[4] P. Berger, J.-P. Katoen, E. Ábrahám, M. T. B. Waez, and T. Rambow. Verifying Auto-generated C Code from Simulink. In *the International Symposium on Formal Methods*, pages 312–328. Springer, 2018.

[5] H. Bourbouh, P.-L. Garoche, T. Loquen, É. Noulard, and C. Pagetti. CoCoSim, a Code Generation Framework for Control/Command Applications: An Overview of CoCoSim for Multi-Periodic Discrete Simulink Models. In *the 10th European Congress on Embedded Real Time Software and Systems*, Toulouse, France, 2020.

[6] O. Burkacky, J. Deichmann, G. Doll, and C. Knochenhauer. Rethinking Car Software and Electronics Architecture. *McKinsey & Company*, 2018.

[7] O. Burkacky, J. Deichmann, and J. P. Stein. Automotive Software and Electronics 2030: Mapping the Sector's Future Landscape. *McKinsey & Company*, 2019.

[8] A. Canedo, J. Wan, and M. A. Al Faruque. Functional Modeling Compiler for System-level Design of Automotive Cyber-Physical Systems. In *2014 IEEE/ACM International Conference on Computer-Aided Design (ICCAD)*, pages 39–46, 2014.

[9] P. Caspi, A. Curic, A. Maignan, C. Sofronis, S. Tripakis, and P. Niebert. From Simulink to SCADE/Lustre to TTA: A Layered Approach for Distributed Embedded Applications. In *LCTES*, page 10, 2003.

[10] W. Chang, D. Roy, L. Zhang, and S. Chakraborty. Model-Based Design of Resource-Efficient Automotive Control Software. In *the IEEE/ACM International Conference on Computer-Aided Design (ICCAD)*, pages 1–8, Nov 2016.

[11] Z. Cheng, R. West, and C. Einstein. End-to-End Analysis and Design of a Drone Flight Controller. *IEEE Transactions on Computer-Aided Design of Integrated Circuits and Systems*, 37(11):2404 – 2415, Nov 2018.

[12] Cincoze. DX1100. https://www.cincoze.com/, 2021.

[13] A. Crespo, I. Ripoll, and M. Masmano. Partitioned Embedded Architecture Based on Hypervisor: The XtratuM Approach. In *the European Dependable Computing Conference*, pages 67–72, 2010.

[14] M. Danish, Y. Li, and R. West. Virtual-CPU Scheduling in the Quest Operating System. In *the 17th IEEE Real-Time and Embedded Technology and Applications Symposium*, pages 169–179. IEEE, 2011.

[15] A. Davare, Q. Zhu, M. Di Natale, C. Pinello, S. Kanajan, and A. Sangiovanni-Vincentelli. Period Optimization for Hard Real-time Distributed Automotive Systems. In *Proceedings of the 44th Annual DAC*, 2007.

[16] D. de Niz, G. Bhatia, and R. Rajkumar. Model-Based Development of Embedded Systems: The SysWeaver Approach. In *the 12th IEEE Real-Time and Embedded Technology and Applications Symposium (RTAS)*, pages 231–242, Apr. 2006.

[17] P. Devanbu, P.-L. Fong, and S. G. Stubblebine. Techniques for Trusted Software Engineering. In *Proceedings of the 20th International Conference on Software Engineering*, pages 126–135. IEEE, 1998.

[18] M. Dürr, G. V. D. Brüggen, K.-H. Chen, and J.-J. Chen. End-to-end Timing Analysis of Sporadic Cause-effect Chains in Distributed Systems. *ACM Transaction on Embedded Computing Systems (TECS)*, 18(5s):1–24, 2019.

[19] B. Finkbeiner, G. Pu, and L. Zhang, editors. *Formal Verification of Simulink/Stateflow Diagrams*, volume 9364 of *Lecture Notes in Computer Science*. Springer International Publishing, Cham, 2015.

[20] B. Fons-Albert, H. Usach-Molina, J. Vila-Carbo, and A. Crespo-Lorente. Development of Integrated Modular Avionics Application Based on Simulink and XtratuM. In *Data Systems In Aerospace*, volume 720, page 15, Aug. 2013.

[21] J. Friedman. MATLAB/Simulink for Automotive Systems Design. In *the Design Automation Test in Europe Conference*, volume 1, pages 1–2, Mar. 2006.

[22] A. Golchin, S. Sinha, and R. West. Boomerang: Real-Time I/O Meets Legacy Systems. In *IEEE RTAS*, pages 390–402, 2020.

[23] Intel. Benefits of ECU Consolidation. 2020.

[24] Z. Jiang, S. Zhao, P. Dong, D. Yang, R. Wei, N. Guan, and N. Audsley. Re-thinking Mixed-criticality Architecture for the Automotive Industry. In *IEEE ICCD*, pages 510–517, 2020.

[25] J. Koshy. libelf by Example, 2010. http://people.freebsd.org/jkoshy/download/libelf/article.html.

[26] Kvaser. https://www.kvaser.com/product/kvaser-usbcan-pro-5xhs/, 2022.

[27] J. Lelli, G. Lipari, D. Faggioli, and T. Cucinotta. An Efficient and Scalable Implementation of Global EDF in Linux. In *OSPERT*, pages 6–15, 2011.

[28] Linux. fexecve - Execute Program Specified via File Descriptor, 2022. https://man7.org/linux/man-pages/man3/fexecve.3.html.

[29] Linux. memfd_create - Create an Anonymous File, 2022. https://man7.org/linux/man-pages/man2/memfd_create.2.html.

[30] C. L. Liu and J. W. Layland. Scheduling Algorithms for Multiprogramming in a Hard Real-time Environment. *Journal of the ACM (JACM)*, 20(1):46–61, 1973.

[31] H. Lu. ELF: From The Programmer's Perspective, 1995.

[32] MathWorks. Block Target File Methods, 2022. https://www.mathworks.com/help/rtw/tlc/block-target-file-methods.html.

[33] MathWorks. Call Custom C/C++ Code from the Generated Code, 2022. https://www.mathworks.com/help/coder/ug/call-cc-code-from-matlab-code.html.

[34] MathWorks. Create a Basic C MEX S-Function, 2022. https://www.mathworks.com/help/simulink/sfg/example-of-a-basic-c-mex-s-function.html.

[35] MathWorks. Create Block Masks, 2022. https://www.mathworks.com/help/simulink/block-masks.html.

[36] MathWorks. Generate Source and Header Files with a Custom File Processing (CFP) Template, 2022. https://www.mathworks.com/.

[37] MathWorks. Simulink Desktop Real-time, 2022. https://www.mathworks.com/products/simulink-desktop-real-time.html.

[38] MathWorks. Spawn Task Function as Separate Linux Thread, 2022. https://www.mathworks.com/help/supportpkg/armcortexa/ref/linuxtask.html.

[39] MathWorks. Using Function-Call Subsystems, 2022. https://www.mathworks.com/help/simulink/ug/using-function-call-subsystems.html.

[40] B. Meenakshi, A. Bhatnagar, and S. Roy. Tool for Translating Simulink Models into Input Language of a Model Checker. In *Formal Methods and Software Engineering*, volume 4260, pages 606–620. Springer Berlin Heidelberg, Berlin, Heidelberg, 2006.

[41] Mercedes-Benz. MB.OS is the "Next Big Thing" - Interview with Dr. Michael Hafner, 2022. https://group.mercedes-benz.com/careers/about-us/mercedes-benz-operating-system/michael-hafner.html.

[42] C. Miller and C. Valasek. Adventures in Automotive Networks and Control Units. *Def Con*, 21:260–264, 2013.

[43] Newlib. The Newlib Homepage, 2022. https://sourceware.org/newlib/.

[44] C. Pagetti, J. Forget, H. Falk, D. Oehlert, and A. Luppold. Automated Generation of Time-Predictable Executables on Multicore. In *the 26th ACM International Conference on Real-Time Networks and Systems*, pages 104–113, France, Oct. 2018.

[45] C. Pagetti, D. Saussié, R. Gratia, E. Noulard, and P. Siron. The ROSACE Case Study: From Simulink Specification to Multi/Many-Core Execution. In *the 19th IEEE RTAS*, pages 309–318, Apr. 2014.

[46] R. Ramsauer, J. Kiszka, D. Lohmann, and W. Mauerer. Look Mum, No VM Exits! (Almost). *arXiv preprint arXiv:1705.06932*, 2017.

[47] F. Reghenzani, G. Massari, and W. Fornaciari. The Real-time Linux Kernel: A Survey on PREEMPT_RT. *ACM Computing Surveys (CSUR)*, 52(1):1–36, 2019.

[48] R. Reicherdt and S. Glesner. Formal Verification of Discrete-Time MATLAB/Simulink Models Using Boogie. In *Software Engineering and Formal Methods*, volume 8702, pages 190–204. Springer International Publishing, Cham, 2014.

[49] D. Roy, M. Balszun, T. Heurung, S. Chakraborty, and A. Naik. Waterfall Is Too Slow, Let's Go Agile: Multi-domain Coupling for Synthesizing Automotive Cyber-Physical Systems. In *ICCAD*, pages 1–7, Nov. 2018.

[50] J. M. Rushby. Design and Verification of Secure Systems. *ACM SIGOPS Operating Systems Review*, 15(5):12–21, 1981.

[51] K. Shigematsu, T. Sekisue, and K. Tsuji. The Automotive System Simulation by Using Multi Domain Modeling Technique. In *2007 European Conference on Power Electronics and Applications*, pages 1–8, Sept. 2007.

[52] H. Simpson. Four-slot Fully Asynchronous Communication Mechanism. *IEEE Computers and Digital Techniques*, 137:17–30, January 1990.

[53] Simulink. Extending Embedded and Generic Real-Time System Target Files, 2022. https://www.mathworks.com/help/physmod/simscape/ug/extending-embedded-and-generic-real-time-targets.html.

[54] S. Sinha, A. Golchin, C. Einstein, and R. West. A Paravirtualized Android for Next Generation Interactive Automotive Systems. In *Proceedings of HotMobile*, pages 50–55, 2020.

[55] S. Sinha and R. West. Towards an Integrated Vehicle Management System in DriveOS. *ACM TECS*, 20(5s):1–24, 2021.

[56] J. Sommer and R. Blind. Optimized Resource Dimensioning in an Embedded CAN-CAN Gateway. In *the International Symposium on Industrial Embedded Systems*, pages 55–62. IEEE, 2007.

[57] B. Sprunt, L. Sha, and J. Lehoczky. Scheduling Sporadic and Aperiodic Events in a Hard Real-time System. Technical report, Carnegie-Mellon University, Pittsburgh, PA, Software Engineering Institute, 1989.

[58] R. West, Y. Li, E. Missimer, and M. Danish. A Virtualized Separation Kernel for Mixed-Criticality Systems. *ACM Transactions on Computer Systems*, 34(3):8:1–8:41, June 2016.

[59] R. Wilhelm, J. Engblom, A. Ermedahl, N. Holsti, S. Thesing, D. Whalley, G. Bernat, C. Ferdinand, R. Heckmann, T. Mitra, et al. The Worst-case Execution-time Problem – Overview of Methods and Survey of Tools. *ACM Transactions on Embedded Computing Systems (TECS)*, 7(3):1–53, 2008.

[60] Wind River. VxWorks | Real-Time Operating System (RTOS), 2022. https://www.windriver.com/products/vxworks.